

Investigation on Conical Vortex Chamber and Channel of Different Parameters

Shahadat Hossain Zehad, Sadman Al Faiyaz, Asilul Kamal, M. A. Mehedi Hasan, Irfan Ahmed

Department of Mechanical Engineering, Bangladesh Army University of Science and Technology, Saidpur 5311, Bangladesh
Faculty of Engineering and Applied Science (Energy Systems Engineering), Memorial University of Newfoundland, St. John's, Newfoundland and Labrador A1C 5S7, Canada

Department of Mechanical Engineering, Khulna University of Engineering & Technology, Khulna 9203, Bangladesh
Department of Mechanical Engineering, Chittagong University of Engineering & Technology, Chattogram 4349, Bangladesh
Email address: shahadathossain01798@gmail.com, alfaiyaz22@gmail.com, asilulkamal.kuet@gmail.com, mamehedi051@gmail.com, irfan_ahmed@baust.edu.bd

Abstract— Extraction of power by means of gravitational vortex generation is one of the most efficient ways to harness energy from the water available in low heads where a vortex generator is used to generate a sufficient amount of vortex which will be capable enough to rotate the vortex turbine. This study has been conducted regarding the geometry of two vortex setup models where the effective model of gravitational vortex setup has to be elected. Two models of vortex setup have been designed in SolidWorks by changing the geometrical parameters of the channel and keeping the dimensions of the vortex chamber alike and several numerical investigations have been carried out with these two models by ANSYS Fluent where the most efficient geometrical setup of vortex generator has been observed by observing the pressure loss and by going through the consideration of multiple fluid flow parameters and flow fields so that the obtained efficient setup model can be taken for further experimental fabrication where observations regarding vortex turbine placement can be examined in an explicit way.

Keywords— Air-Core, Pressure, Pressure Loss, Swirling Strength, Velocity, Vortex.

I. INTRODUCTION

In the power generation sector, hydro-power plays an important role. Power is being extracted from the water source in several methods at different heads. However, there are a plethora of places on earth where water flow is available at low heads. To extract power from the flow of water from those heads, vortex technology has been introduced. Water flow generates vortex motion which is the circulatory motion caused by the rotating mass of fluid at the vortex chamber, which is sufficient enough to rotate the blades of the vortex turbine that has been placed in the vortex chamber at a suitable position. Regarding gravitational vortex generation, some researches have been carried out. Wanchat and Suntivarakorn (2011) investigated the most suitable arrangement for a gravitational water vortex pool in a vortex chamber of cylindrical shape where the outlet section has been set centrally at the bottom [1]. J. A. Chattha,

T. A. Cheema, and N. H. Khan explained the most favorable parameters of a vortex generator for the generation of a strong vortex to improve the efficiency of gravitational water vortex turbine [2]. The effect on vortex formation propagating from the conical basin by analyzing multiple geometrical parameters has been described by Dhakal et al. (2014) [3]. This study has been extended from the investigation carried out by Zehad et al. (2021) where an explanation has been made regarding the cylindrically shaped vortex chamber of different mensuration to observe the strongest vortex formation based on several flow fields [4]. The extended study involves further modification on the vortex chamber along with the attached channel that exhibits less amount of pressure loss to extract

further productive vortex generator which can able to rotate the gravitational vortex turbine more efficiently by investigating through the pressure losses within the tunnel and vortex chamber and observing from the flow fields that include the pressure and velocity profile of the channel, vortex chamber and the strength of swirl and rendered velocity from the vortex core.

II. METHODOLOGY

From the conclusion of the research carried out by Zehad et al. (2021), it has been observed that two vortex chambers of different geometries have been taken under experiments where the vortex chamber through which the strongest vortex formation has been generated has been brought up under the investigation through several flow fields. After taking the selected model of that vortex chamber for further investigation, it has been seen that the vorticity renders a good amount of pressure loss within that selected vortex chamber through which energy might not be extracted up to the requirement after vortex turbine placement. To minimize the pressure loss for efficient vortex formation, two new models of vortex generator are being designed in this study of conical shape concerning the model of the vortex chamber that renders less amount of pressure loss described in the research conducted by Zehad et al. (2021) [4].

A. Designed Model

Two new vortex chambers are modeled of conical-shaped geometry to investigate the effects on vorticity for bringing out the efficient vortex generation. The geometry of model-1 has

the conically shaped vortex chamber with the tunnel where the posterior section of the tunnel has been contracted so that the speed water flow accelerates rapidly and enters the vortex chamber. On the flip side, the geometry of the tunnel has been modeled in a rectangular shape by keeping the same geometrical parameters of the vortex chamber for model-2 where no contraction at the outlet section of the tunnel has been given. Both of the models have been designed by SolidWorks using necessary geometrical parameters and syntaxes

TABLE 1. Geometrical parameters of two models

S. No.	Different positions of vortex chamber	Model-1 (m)	Model-2 (m)
1	Chamber Diameter	1.5	1.5
2	Chamber Height	1.5	1.5
3	Tunnel Height	0.4	0.4
4	Tunnel Inlet Width	0.28	0.5
5	Diameter of the Outlet	0.15	0.15

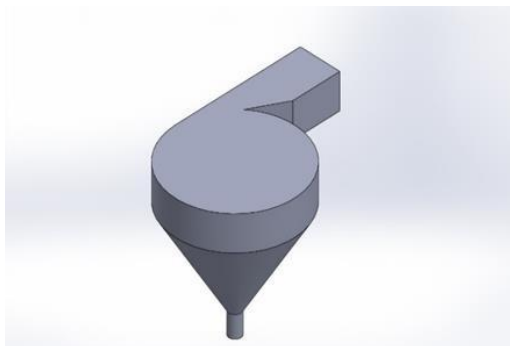


Fig. 1. CAD Modeling of the Fluid Domains of Model-1

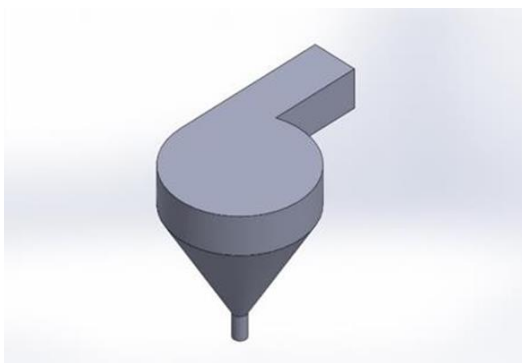


Fig. 2. CAD Modeling of the Fluid Domains of Model-2

B. Mathematical Modelling

The air-core vortex was studied using the parameters of stable, axisymmetric, and incompressible flow. The continuity equation and the Navier-Stokes equations for cylindrical coordinates are given below [3]:

ANSYS CFD Fluent was utilized to deal with the problems because solving the above equations analytically is quite challenging and complicated as well. The fluid flow domain was designed as indicated in figure 1 and figure 2 for simulation purposes that use the SolidWorks software. The model was then simulated using ANSYS Fluent under observation through several flow parameters.

$$\frac{\partial v_r}{\partial r} + \frac{\partial v_z}{\partial z} + \frac{v_r}{r} = 0 \tag{1}$$

$$\partial V_r \frac{\partial v_\theta}{\partial r} + V_z \frac{\partial v_\theta}{\partial z} - \frac{v_r v_\theta}{r} = \nu \left(\frac{\partial^2 v_\theta}{\partial r^2} + \frac{\partial v_\theta}{r \partial r} - \frac{v_\theta}{r^2} + \frac{\partial^2 v_\theta}{\partial z^2} \right) \tag{2}$$

$$V_r \frac{\partial v_r}{\partial r} + V_z \frac{\partial v_r}{\partial z} - \frac{v_\theta^2}{r} + \frac{\partial \rho}{\rho \partial r} = \nu \left(\frac{\partial^2 v_r}{\partial r^2} + \frac{\partial v_r}{r \partial r} - \frac{v_r}{r^2} + \frac{\partial^2 v_r}{\partial z^2} \right) \tag{3}$$

$$\partial V_r \frac{\partial v_z}{\partial r} + V_z \frac{\partial v_z}{\partial z} + \frac{\partial \rho}{\rho \partial z} = g + \nu \left(\frac{\partial^2 v_z}{\partial r^2} + \frac{\partial v_z}{r \partial r} + \frac{\partial^2 v_z}{\partial z^2} \right) \tag{4}$$

C. Numerical Analysis

Before going through numerical simulation, these two models of different geometrical parameters have been taken under a mesh generator where the models have meshed exquisitely as possible. Both of the models have meshed by tetrahedral elements in order to fit properly in the entire geometry. Model-1 has been meshed by 505973 elements with 99217 nodes whereas model-2 has been meshed by 510534 elements along with 100030 nodes.

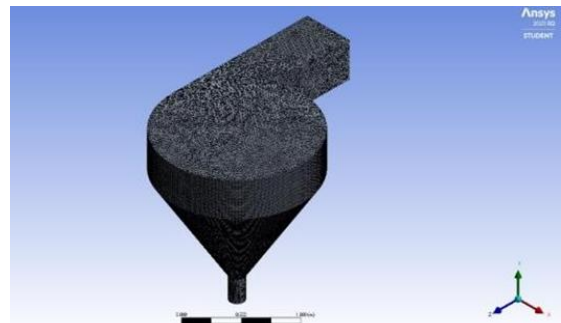


Fig. 3. Generated Mesh of Model-1

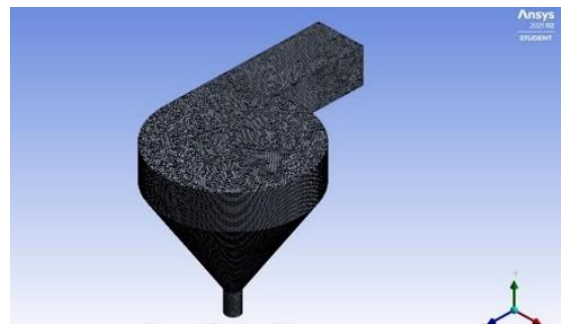


Fig. 4. Generated Mesh of Model-1

As for the boundary conditions, the simulation was conducted by SIMPLE algorithm for solving the Navier–Stokes equations. Taking the viscous model of k-epsilon standard, steady-state condition has been set for the flow of water. The inlet boundary condition has been taken as velocity inlet at 1.8 m/s and pressure outlet taking the gauge pressure at 0 Pa as for the outlet boundary condition. The number of iterations has been set at 5000 where all the residual convergence conditions have been taken at 1e-4 for both models [4]. The results of the simulations have been investigated further to observe the outcomes.

III. RESULT AND DISCUSSION

By observing the two cases of vortex chambers studied in Zehad et al. (2021), the vortex chamber that generates potent vorticity renders a high amount of pressure loss compared to the other case [4]. To surpass the matter, two new models have been designed by taking reference from the model that exhibits less amount of pressure loss explained in Zehad et al. (2021) from which further investigations has been carried out to bring out the efficient vortex generator on the basis of pressure losses and several flow parameters.

A. Pressure Loss

In terms of calculating the pressure loss, two vortex chamber models have been divided by different sections named channel section, vortex chamber section and outlet pipe section respectively. Now by exporting the data of pressure losses through numerical simulation by taking mass flow average at different sections of vortex chamber of both models, it has been noticed that model-1 generates more total pressure loss than model-2 that has been shown in figure 5. From the section of the vortex chamber, it is noticeable that the loss in model-1 is almost three times greater than the loss generated in model-2. Despite experiencing sudden expansion by the fluid particles, pressure loss at model-1 is more due to the contracted area at the outlet section of the channel which results in a high amount of sudden expansion ratio. As model-2 has a rectangular channel by having the same width in both inlet and outlet sections, the sudden expansion ratio is less than model-1 which mainly differentiates the amount of pressure losses between both models.

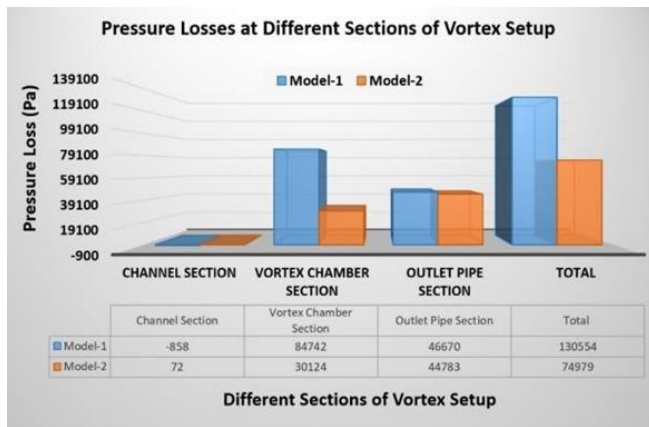


Fig. 5. Pressure Losses for Both Models

B. Effect on Channel

Figure 6 and figure 7 illustrates the behavior of static pressure drop at the channel sections of both models. It has been clearly noticed that both of the static pressure curves of model-1 and model-2 have been decreasing gradually from the inlet towards the outlet section. Due to having a contraction section at the posterior end of the model-1 channel section, static pressure drops out there rapidly whereas the model-2 channel section exhibits a less amount of static pressure loss due to not having any sudden contraction area at the outlet region of the channel.

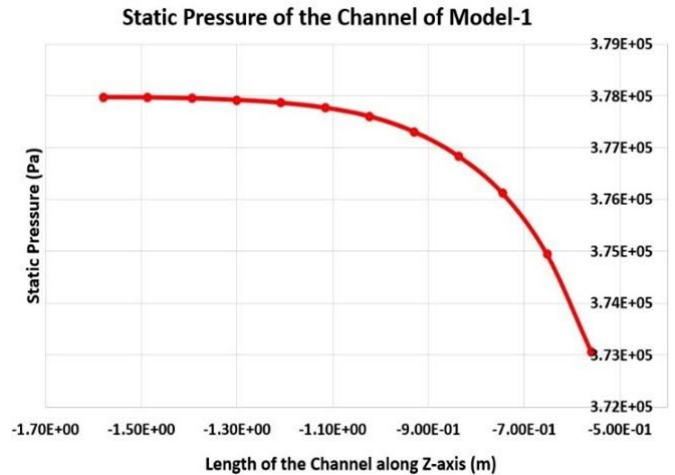


Fig. 6. Static Pressure of the Channel for Model-1

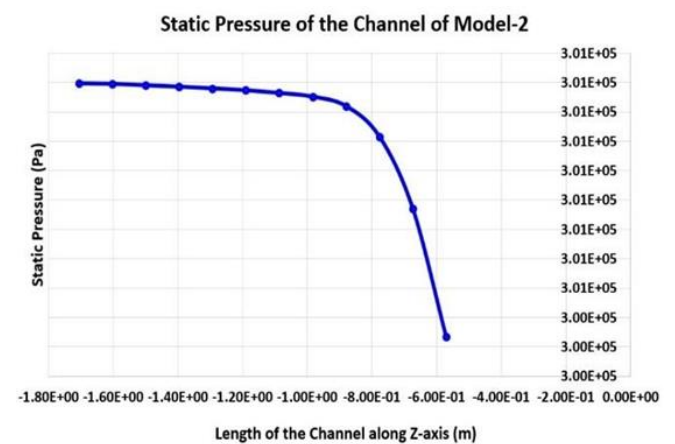


Fig. 7. Static Pressure of the Channel for Model-2

The behavior of total pressure at the channel section for both model-1 and model-2 has been observed from the figures 8 and 9 where two different phenomena have been noticed here. The total pressure of at channel of model-2 gradually decreases along with the length of the channel along with the fluid flow towards the outlet section. But a different visibility has been developed in terms of model-1 during the fluid flow from inlet to the outlet section. At the contraction portion of the channel of model-1, the overall pressure has been raised slightly. Due to the contracted portion at the outlet section of the channel, the particles of fluid that are flowing towards the outlet section collide with the contracted region's walls, where the fluid particle's velocity becomes almost zero, thus results in an increase in total pressure in the stagnation region [5].

Effect on velocity has been observed at the channel of both the models that have been depicted in figure 10 and figure 11. With the flow of the fluid particles, the velocity increases gradually while approaching the outlet section of the channel for both models. Because of the contracted geometrical shape at the outlet section of the channel of model-1, velocity accelerates rapidly at the outlet region of the channel whereas model-2 doesnot generate that much velocity as model-1 due to having a rectangular geometrical shaped channel.

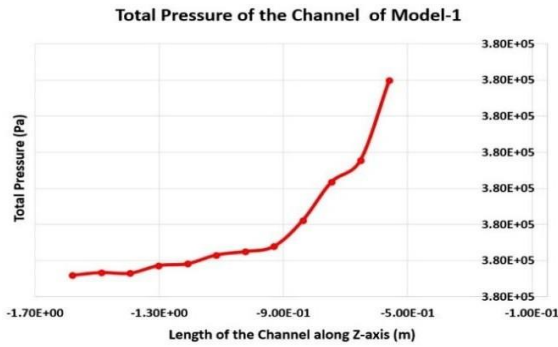


Fig. 8. Total Pressure of the Channel for Model-1

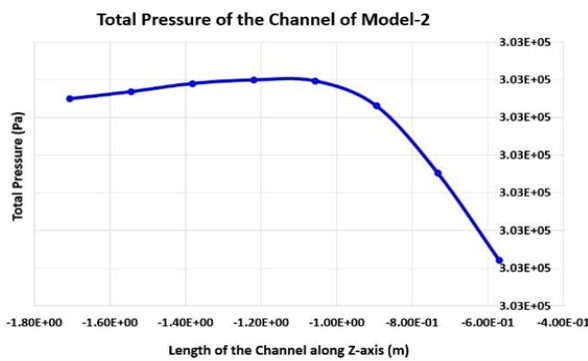


Fig. 9. Total Pressure of the Channel for Model-2

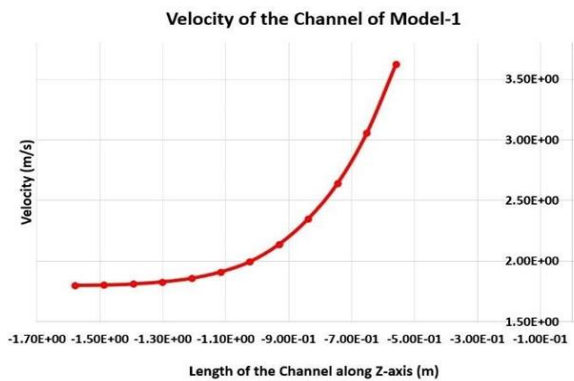


Fig. 10. Velocity of the Channel for Model-1

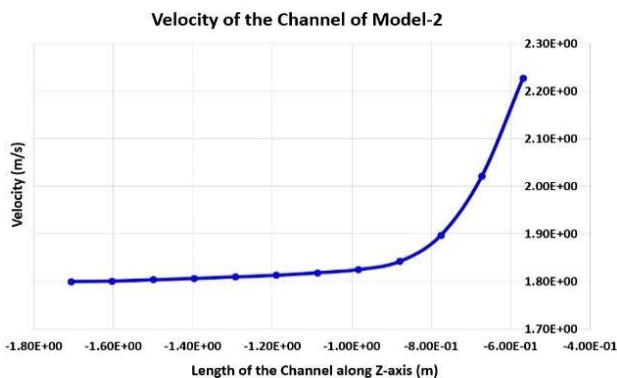


Fig. 11. Velocity of the Channel for Model-2

C. Effect of Velocity on Vortex Chamber

Figure 12 explains how the velocity changes throughout the vortex chamber. As the inlet velocity of the vortex chamber of model-1 is more compared to model-2 due to having a channel

with a contraction portion attached with it, the generated velocity of the vortex formation within the vortex chamber of model-1 has been found more than model-2. Velocity curve of both models have been increased steeply while the fluid flow reaches near the bottom of the vortex chamber. However, the velocity for model-2 has been accelerated before model-1 which indicates that the length of the air-core formed within the vorticity at model-2 is less than model-1 due to less amount of velocity within the formation of vortex as there is no contraction portion at the end section of the channel attached with the vortex chamber of model-2.

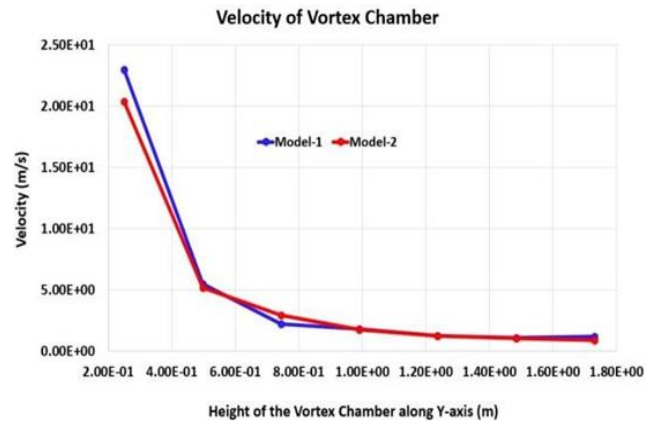


Fig. 12. Velocity of the Channel for Model-2

D. Effect of Pressure on Vortex Chamber

Figure 13 and 14 illustrates the static and total pressure within the vortex chamber for model-1 and model-2 respectively. It has been observed that the level of the static and total pressure of model-1 decelerates rapidly than model-2. Due to the high amount of sudden expansion, the fluid particles encounter a sudden change of direction, resulting in a high amount of pressure loss. As the channel of model-1 has a contraction portion at the end section, it allows the fluid particles to generate more velocity within the vortex chamber but ends up in a greater amount of pressure drop in terms of both static and total pressure compared to model-2. As a result, the total pressure drop has been steeper in the case of model-1 than model-2.

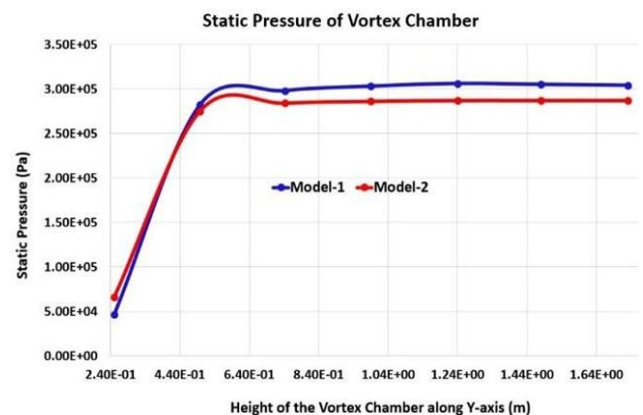


Fig. 13. Static and Total Pressure of the Vortex Chamber for Model-1

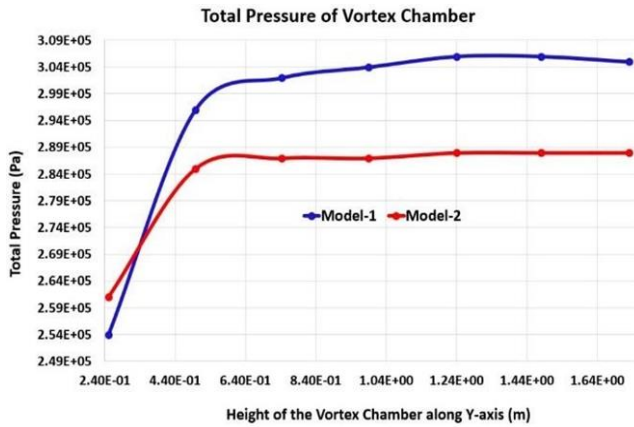


Fig. 14. Static and Total Pressure of the VortexChamber for Model-2

E. Effect on Outlet Pipe Section

Figure 15 and figure 16 shows the behaviors of the static and total pressure of the outlet pipe section from the inlet to the outlet for model-1 and model-2. There is a common phenomenon observed in the case of static and total pressure for both the models where the pressure curve gradually decreases while the fluid flow approaches towards the outlet of the outlet pipe section. From the total pressure curve, the pressure drop of model-1 is more than model-2 which has been occurred due to the effect of a huge pressure drop at the vortex chamber section of model-1.

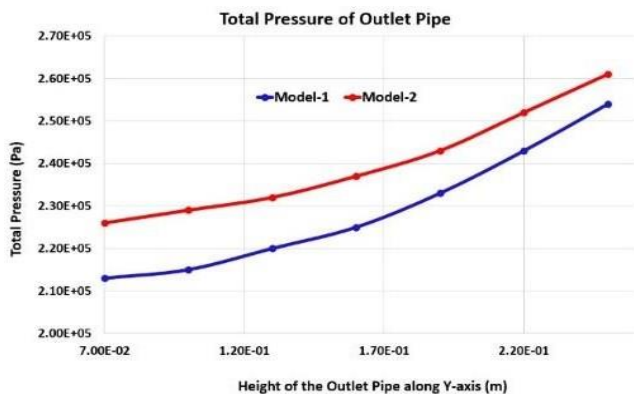


Fig. 15. Static Pressure of the Outlet Pipe Section for both Models

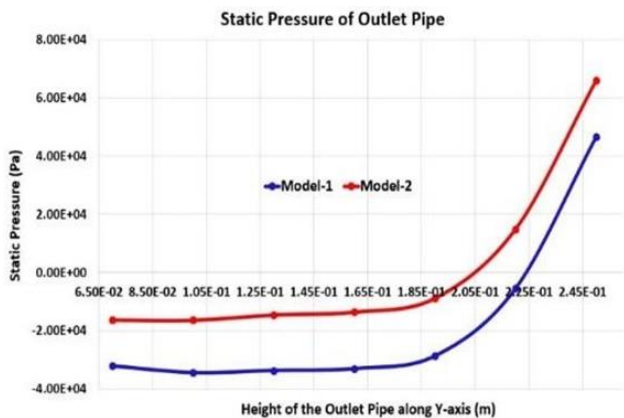


Fig. 16. Total Pressure of the Outlet Pipe Section for both Models

In figure 17 the graphical representation of velocity for the outlet pipe section of both models has been shown. It has been noticed that the velocity of model-1 has been generated more than model-2 as the amount of pressure drop has been more in model-1. At a certain height of the outlet pipe section, the velocity acquires its maximum value and after that velocity starts to fall down gradually towards the outlet. This phenomenon has been taken place due to the contraction of the fluid particles while entering the outlet pipe from the outlet section of the vortex chamber where the velocity is maximum along with pressure drop at the outlet pipe section.

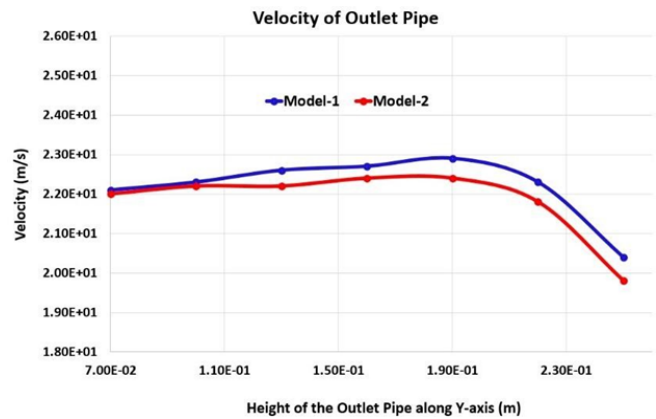


Fig. 17. Velocity of the Outlet Pipe Section for both Models

F. Observation on Vortex Formation

From the above fluid motion and pressure changes at different sections of the two models, it has been found that model-2 generates a more efficient vortex over model-1. Though model-1 renders more velocity and more flow rate at the vortex chamber, it ends up in a huge pressure loss compared to model-2 which will not allow the vortex turbine to extract the required amount of power vortex formation. As a result, model-2 has been taken as an efficient vortex generator from which further examinations have been carried out regarding the formation of vorticity. Figure 18, Figure 19, Figure 20, and Figure 21 represent the velocity contours of model-2 at different angles that have been taken at the XY plane. The contours clearly show the shape of the air-core formed within the vortex formation is different from each angle at the XY plane which indicates the shape of the vortex is unsymmetrical.

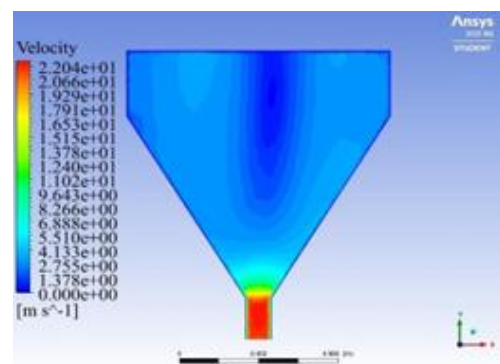


Fig. 18. Velocity Contour in XY Plane at 0° for Model-2

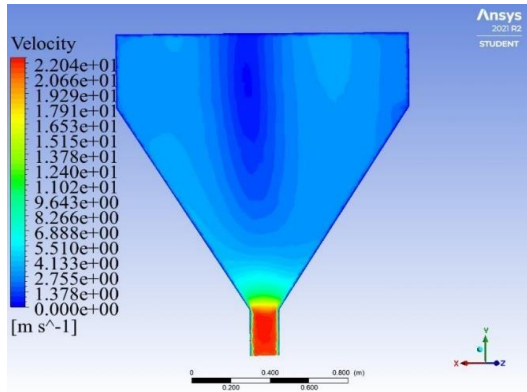


Fig. 19. Velocity Contour in XY Plane at 30° for Model-2

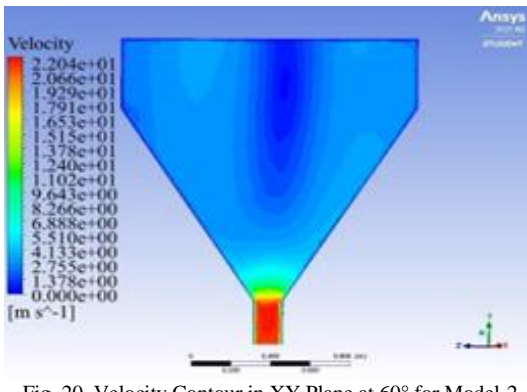


Fig. 20. Velocity Contour in XY Plane at 60° for Model-2

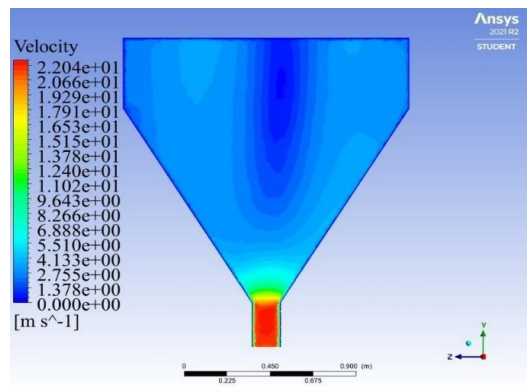


Fig. 21. Velocity Contour in XY Plane at 90° for Model-2

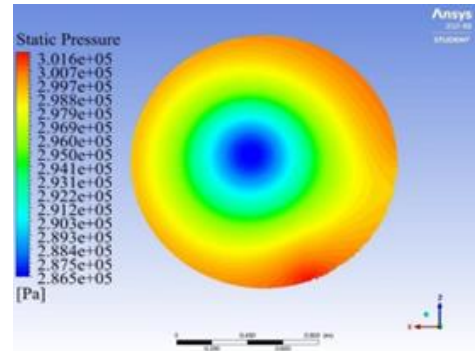


Fig. 22. Static Pressure Contour in ZX Plane at 100% Height from bottom of the vortex chamber for Model-2

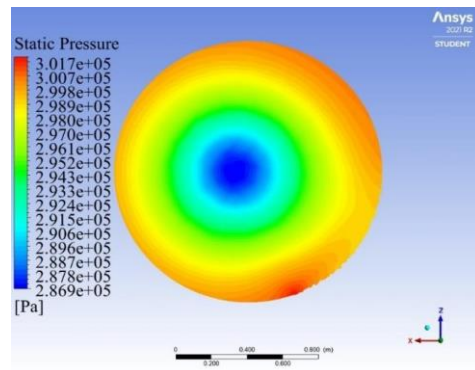


Fig. 23. Static Pressure Contour in ZX Plane at 75% Height from bottom of the vortex chamber for Model-2

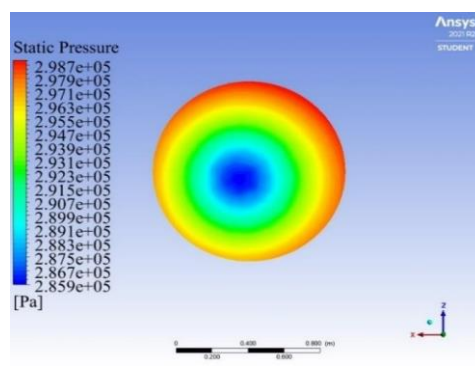


Fig. 24. Static Pressure Contour in ZX Plane at 50% Height from bottom of the vortex chamber for Model-2

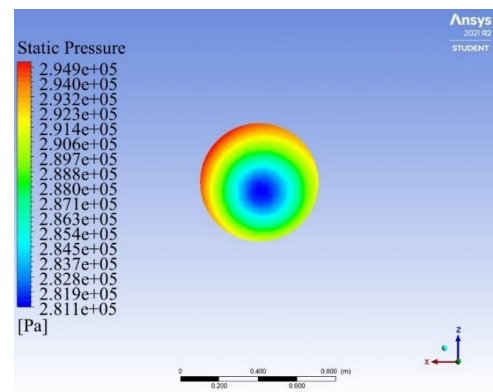


Fig. 25. Static Pressure Contour in ZX Plane at 25% Height from bottom of the vortex chamber for Model-2

The static pressure contours at different heights of the vortex chamber of model-2 have been depicted from figure 22 to figure 26 where 100% indicates the total height of the vortex chamber and 0% indicates the bottom position of the vortex chamber respectively. From these contour plots, the position of air-core formation has been observed where the air-core appears in different positions at different height levels of the vortex chamber. The formation of air-core has been found between 100% to 25% of the height levels and after that, the air-core starts to fade away and does not appear at the bottom level of the vortex chamber.

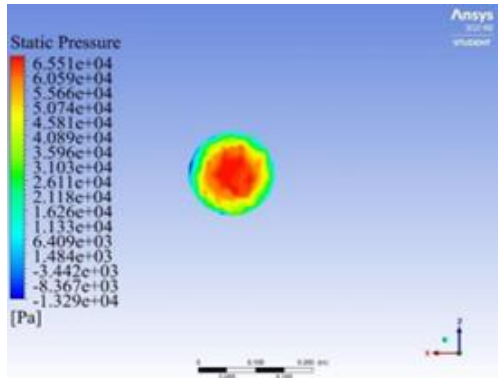


Fig. 26. Static Pressure Contour in ZX Plane at 0% Height from bottom of the vortex chamber for Model-2

IV. CONCLUSION

Differentiation regarding two vortex setups of conical shape including two different geometrical parameters of the channel has been executed in order to bring out the efficient vortex setup. Comparison has been made by keeping the geometrical shape of the vortex chamber and outlet pipe section the same and by changing the outlet section of the channel where it has been clearly observed throughout the investigation that the channel with the contraction section at its outlet section of model-1 renders more pressure loss than the channel with a rectangular shape. Due to a comparative more pressure loss of the contracted channel, the ratio of sudden expansion becomes high that the particles of fluid confront while entering the vortex chamber attached with the contracted channel which results in a high-pressure drop within that chamber during the generation of vorticity. As a consequence, the pressure drop gets increased at the outlet pipe section of model-1. By investigating through pressure losses at different sections of the vortex setup of both models through numerical simulations, model-2 has been found as the most efficient vortex setup. Despite having less velocity generation within the vortex chamber of model-2, the loss of pressure at the vortex chamber is significantly less leading to an effective vortex formation. Further investigations are to be conducted with the efficient model after it gets fabricated.

G. Observation on Swirling Strength and Vortex Core Velocity

Figure 27 and figure 28 shows the strength of the swirl through which a vortex formation can be indicated and the velocity that has been generated within the vortex core formation for model-2. Within the formation of the vortex in model-2, the swirling strength has been obtained 3.45 s^{-1} and the maximum velocity generated within the vortex core has been found 16.3 m/s . A geometrical shape of the air-core formation has been extracted from the numerical simulation where it has been under the visualization that the air-core formation is in the asymmetric shape.

NOMENCLATURE

V_{θ}	Tangential Velocity	ν	Kinematic Viscosity
V_r	Radial Velocity	ρ	Density of Fluid
V_z	Axial Velocity	g	Gravitational Acceleration
r	Radial Distance		

REFERENCES

1. Wanchat, S.; Suntivarakorn, R. Preliminary Design of a Vortex Pool for Electrical Generation. *Journal of Computational and Theoretical Nanoscience*, January 2011, DOI: 10.1166/asl.2012.3855.
2. Chattha, J.A.; Cheema, T.A.; Khan, N.H. Numerical investigation of basin geometries for vortex generation in a gravitational water vortex power plant. 2017 8th International Renewable Energy Congress (IREC), 2017, DOI: 10.1109/IREC.2017.7926028.
3. Dhakal, S.; Timilsina, A.B.; Dhakal, R.; Fuyal, D.; Bajracharya, T.R.; Pandit, H.P. Effect of Dominant Parameters for Conical Basin: Gravitational Water Vortex Power Plant. International Conference on Technology and Innovation Management & IOE Graduate Conference, Kathmandu, Nepal, October 2014, DOI: 10.13140/RG.2.1.1455.7843.
4. Zehad, S.H.; Faiyaz, S.A.; Ahmed, I.; Raihan, A.M. A Comparative Numerical Analysis for Vortex Generation on Different Geometries. Lecture Notes in Engineering and Computer Science: Proceedings of The World Congress on Engineering, 7-9 July 2021, London, U.K., pp262-267, ISBN: 978-988-14049-2-3.
5. Zehad, S.H.; Faiyaz, S.A.; Islam, M.R.; Ahmed, D.-I.I. Numerical Analysis of Gravitational Vortex Chamber. *Technium: Romanian Journal of Applied Sciences and Technology*, vol. 3, no. 10, pp. 11–22, Nov. 2021.

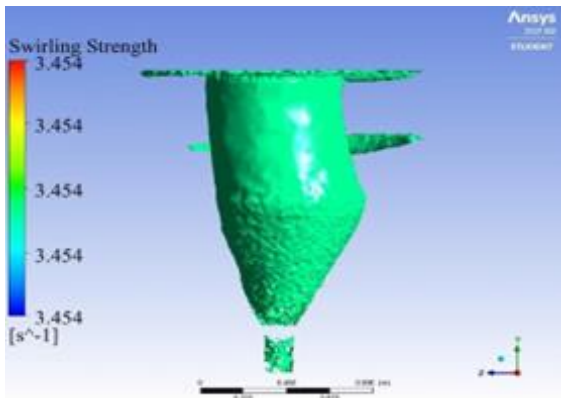


Fig. 27. Swirling Strength for Model-2

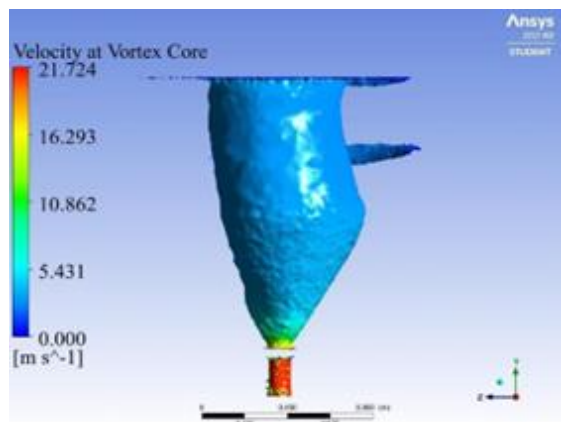


Fig. 28. Vortex Core Velocity for Model-2